J. Fluid Mech. (1987), *vol.* 183, *pp.* 45–62
Printed in Great Britain

Coherent baroclinic eddies on a sloping bottom

By M. MORY,
Institut de Mécanique de Grenoble, BP68, 38402 St Martin d'Hères cédex, France

M. E. STERN
University of Rhode Island, Graduate School of Oceanography, Narragansett, RI 02882, USA

AND R. W. GRIFFITHS
Research School of Earth Sciences, Australian National University,
G.P.O. Box 4, Canberra, 2601, Australia

(Received 19 June 1985 and in revised form 29 January 1987)

A coherent and stable baroclinic eddy in a rotating fluid was produced on a sloping bottom by releasing a dome of salt water into the ambient fresh water. A strong cyclonic vortex is produced above the heavy dome. The entire eddy system moves 'north-westward' (with the up-slope direction designated 'north') as a 'Taylor column'. The eddy system displays long lifetimes, but it is shown that a theory of isolated systems cannot account for the experimental observations. Instead, it is demonstrated that the vortex flow above the lens is along the lines of constant depth, producing a net pressure force on the lens, which approximately balances the buoyancy force. When Ekman friction is also included, it accounts for the northward motion of the dome.

1. Introduction

Evidence that coherent eddies are present and play a key role in the dynamics of the ocean has accumulated, largely from near-surface observations of warm and cold rings in the vicinity of the Gulf Stream (Ring Group 1981). Bottom eddies have also been identified as patches of cold water moving along the coastal slope in the Mid-Atlantic Bight (Houghton *et al.* 1982). Such eddies may result from baroclinic instability of bottom gravity currents (Smith 1976; Griffiths, Killworth & Stern 1982) and they may transport the bulk of the cold bottom water emerging from the Denmark Strait overflow. The evolution and translation of the eddies would then be an important factor in the mixing of the dense water and in determining the time-average structure of the bottom current.

Coherent eddies have weak interactions with the surrounding ocean, and they have been idealized in theoretical models that investigate isolated systems with no momentum transfer to the surrounding fluid. The first model of an isolated and strongly nonlinear geophysical eddy was the modon (Stern 1975*a*; Flierl 1979*a*), which consisted of a cyclone–anticyclone vortex pair. Models for warm- and cold-core rings with circulation in one sense only were later introduced (Flierl 1979*b*). Models of cold eddies on a sloping bottom or a β-plane were given by Nof (1983), Killworth (1983) and Flierl (1984).

Additional insights into such strongly nonlinear systems may be obtained by laboratory experiments. Flierl, Stern & Whitehead (1983) generated barotropic

dipoles and there have been several experiments in which such eddies emerge as a result of baroclinic instability. In the present work we investigate the baroclinic eddy produced by releasing a finite volume of dense fluid on a sloping bottom beneath an upper layer of finite depth. The study was suggested by an unpublished experiment carried out previously by one of the authors (R.W.G.), in which a gravity current is introduced on a parabolic slope in a rotating tank. The current adjusts by moving down-slope until it reaches a depth at which it begins to flow approximately along contours of constant depth. The current was observed to break into a number of coherent baroclinic eddies, involving most of the dense fluid in the resulting bottom current. A surprising feature of these eddies was the presence of an intense cyclonic vortex above each dome of dense water. We have tried to isolate this effect in a much simpler experiment, and to develop a theoretical understanding of it. We show that most of the kinetic energy is in the deep light fluid above the dome, and this distinguishes our work from the models of Nof (1983) and Killworth (1983), who considered the case of cold domes on a sloping bottom beneath an infinitely deep and motionless upper layer.

2. Formulation

Consider the two-layer model shown in figure 1. The lower layer consists of a lens of finite volume with density $\rho+\Delta\rho$ resting on a bottom with linear slope s, and lying beneath a lighter fluid of density ρ. The reference frame (O, X, Y, Z) is stationary with respect to the rotating tank, whereas the frame (A, x, y, z) translates with the lens, and has its origin A at the centre of the eddy. The top surface is limited by a rigid lid, and $H(A)$ designates the total depth of the layer at A. The depths of the upper and lower layers are h_1 and h_2 respectively (subscripts 1 and 2 generally refer to the upper and lower layers, respectively), and are related by

$$h_1(x,y) = H(A) - sy - h_2(x,y). \tag{2.1}$$

We restrict ourselves to steadily east–west propagating domes in which the velocity of the dome centre relative to the tank is denoted by C_x. North–south displacements of the lens would preclude a steady solution.† The system considered here is very like the one studied by Nof (1983), except that the upper layer was infinitely deep and motionless in Nof's model. When motion in the upper layer is taken into account, the pressure $p_2(x,y,z,t)$ in the lens is related by the hydrostatic equation to the pressure anomaly in the upper layer $p_1(x,y,t)$ (relative to (∞,∞,z,t)), i.e.

$$p_2 = p_1 + \Delta\rho g(h_2 + sy - z). \tag{2.2}$$

The momentum equations for the lens in the coordinate system moving with the lens are

$$u_2\partial_x u_2 + v_2\partial_y u_2 - fv_2 = -\frac{1}{\rho}\partial_x p_2 = -\frac{1}{\rho}\partial_x p_1 - \frac{\Delta\rho}{\rho}g\partial_x h_2, \tag{2.3}$$

$$u_2\partial_x v_2 + v_2\partial_y v_2 + fu_2 + fC_x = -\frac{1}{\rho}\partial_y p_2 = -\frac{1}{\rho}\partial_y p_1 - \frac{\Delta\rho}{\rho}g\partial_y h_2 - \frac{\Delta\rho}{\rho}gs. \tag{2.4}$$

† In §4 the momentum equations will be expanded in the small parameter β ($\beta = sL/H$, H and L being the vertical and horizontal lengthscales) in the manner previously carried out by Killworth (1983) and Flierl (1984). The results of the present section will hold, provided that the flow is independent of time at the first and second orders of the β-expansion.

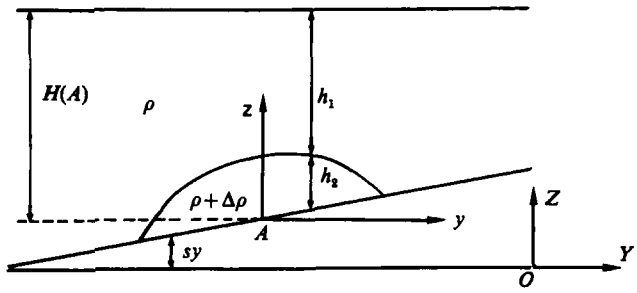

FIGURE 1. A sketch of a lens of dense fluid on a sloping bottom. The coordinate system moving with the lens is (A, x, y, z). The reference frame is (O, X, Y, Z).

On integration of the momentum equations over the entire lens we recover the equations obtained by Nof (1983) with an additional pressure force applied on the lens by the vortex above it. Thus

$$O = -\iint_{\mathscr{S}} h_2 \partial_x p_1 \, dx \, dy, \tag{2.5}$$

$$fC_x \iint_{\mathscr{S}} h_2 \, dx \, dy = -\iint_{\mathscr{S}} h_2 \partial_y p_1 \, dx \, dy - \frac{\Delta\rho}{\rho} gs \iint_{\mathscr{S}} h_2 \, dx \, dy, \tag{2.6}$$

where $\mathscr{S}$ denotes the area in the plane (x, y) covered by the dome. The translation speed of the dome then depends on the motion in the upper layer. In Nof's (1983) theory the overlying deep fluid was assumed to be at rest, and the translation speed (denoted C_1) is therefore

$$C_1 = \frac{-\Delta\rho g s}{\rho f}. \tag{2.7}$$

The case of isolated eddies is of special interest for oceanic applications because they do not radiate energy by Rossby waves. This may explain the persistence of some eddies in the ocean, and some features of the eddy system produced in our experiment (long lifetime, coherency and strong vorticity above the lens). If the eddy system in figure 1 is isolated, and if $p_1(x, y, t)$ denotes the pressure anomaly (relative to $x = \infty$) on the upper surface, then the integrated momentum equations imply (Mory 1985):

$$\iint_{-\infty}^{+\infty} (p_1 + \Delta\rho g h_2) \, dx \, dy = 0. \tag{2.8}$$

Thus the average pressure above the heavy dome is negative and proportional to the volume of the dome. An important consequence of (2.8) is the prediction of strong cyclonic motions above the lens, an effect that is observed in the previously cited (R. W. G.) experiment as well as in the experiment presented below. Nof (1985) recently claimed that the lateral scale of the motions above the lens depends on the external radius of deformation. We disagree with this statement because the rigid-lid approximation is irrelevant to the existence of isolated eddies so that the external radius of deformation is irrelevant and the lateral scales of the motions above and in the lens are the same. However, we should expect some motion to occur on the scale of the external radius of deformation, especially when an eddy is produced, but they are observed to be weak and unimportant in the experiments presented in this paper. Equation (2.8) does not require the eddy to be steadily propagating, nor does

it restrict the depth of the upper-layer fluid. However, the integral constraint (2.8) has very strong implications in terms of the kinematics of the flow. It requires two assumptions concerning the decay of the solution far away from the eddy. The pressure p_1 and the velocity v_1 have to decrease faster than $1/r^2$ as $r \to \infty$ (Mory 1983). It is shown in §4 that the eddy produced in the experiment is not isolated because it does not satisfy the integral theorem (2.8).

Another indication that the eddy produced in the experiment is not isolated will follow from (2.7). The velocity C_i is also the translation speed of isolated eddies even in the presence of strongly nonlinear motion above the lens. If the magnitude of the motion within the lens is sufficiently small, the geostrophic balance holds within the lens (note that the front at the edge of the lens precludes the use of quasi-geostrophic theory in the lens):

$$\left.\begin{aligned} -\rho f v_2 &= -\partial_x p_2, \\ \rho f u_2 + \rho f C_x &= -\partial_y p_2, \end{aligned}\right\} \tag{2.9}$$

u_2 and v_2 being the velocities in the moving coordinate system. Since the edge of the lens is a streamline in the moving coordinate system, we get

$$p_2 + \rho C_x f y = \text{const} \tag{2.10}$$

along that line. The comparison of the latter relationship with the hydrostatic equation (2.2) shows that the pressure p_1 in the upper layer depends on y at the edge of the lens if the translation speed departs from C_i (2.7), implying that Rossby waves are generated outside the eddy.

3. The laboratory model

3.1. *The experiment*

The experimental set-up is shown in figure 2. Experiments were conducted in a square tank (108 cm wide) mounted on a rotating table. The table was rotated at a constant rate $\Omega = \frac{1}{2}f$ between 0.8 and 1.25 rad s^{-1}. A plate was placed on the bottom of the tank at an angle of $\alpha \approx 8°$ with the horizontal plane. The bottom slope was then $s \approx 0.14$. The tank was filled with fresh water and a dense lens was produced by suddenly releasing a finite amount of salt water on the bottom in the manner previously used by Saunders (1973) and Griffiths & Linden (1981). Before starting the experiment the dense fluid was held in an upright cylinder (diameter R_0) on the bottom and occupied a depth $\delta_0 H$ (H being the total depth of the water at the centre of the cylinder). Small holes through the cylinder slightly below the free surface permitted an equalization of surface height inside and outside the cylinder as the salt water was added. The relative density difference $\Delta\rho/\rho$ between the fresh and the saline fluids ranged from 0.45% to 0.65%. Experiments were started by pulling up the cylinder. Under the action of buoyancy forces the heavy fluid then began to spread out on the bottom, producing compression of fluid columns in the lens and stretching in the fluid above the lens. Within a few rotation periods the motion evolved towards a balanced cyclonic circular vortex. Observations show that the dense fluid spreads through approximately one deformation radius $R_d = (g'H)^{\frac{1}{2}}/f$, in agreement with previous measurements by Saunders (1973). The typical diameter $2L$ of the lens is

$$2L \approx 2(R_0 + R_d). \tag{3.1}$$

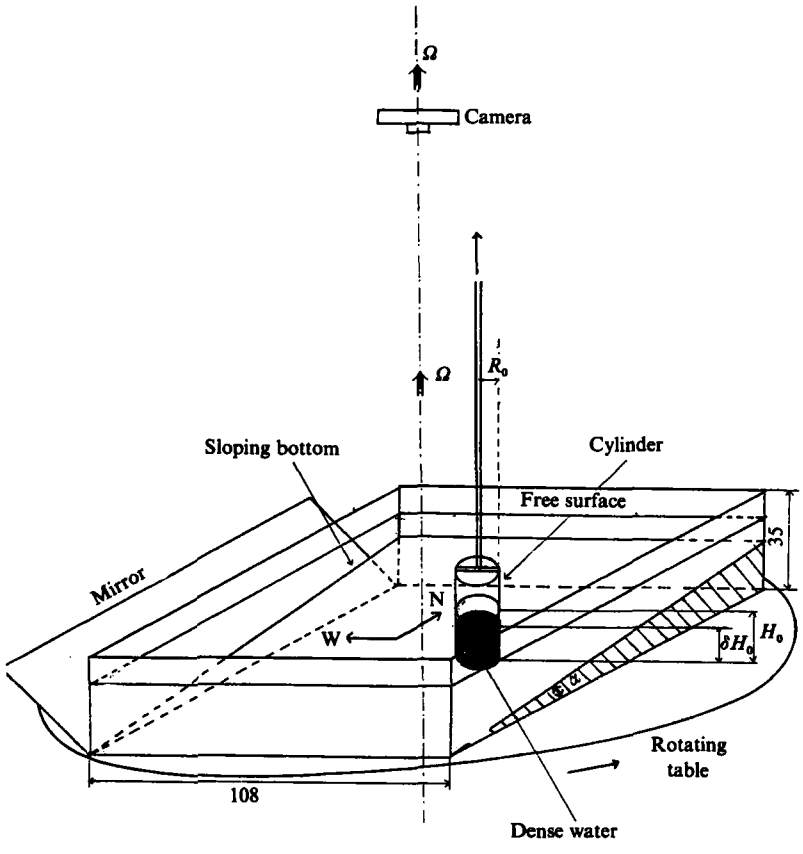

FIGURE 2. Schematic diagram of the experimental set-up.

All direct measurements were made from photographs taken by a camera fixed above the tank and rotating with the table, and successive exposures revealed the displacement of the dyed lens of heavy fluid. In addition to the plan view, the side view of the lens was recorded on each photograph through an inclined mirror placed alongside the tank. In some experiments fluoresceine dye was mixed with the upper layer fluid in the cylinder before starting the experiment, and this revealed the subsequent motion of the upper layer. The displacements of small paper pellets lying on the free surface, as revealed by exposures of 5 s duration, were also used to estimate the instantaneous velocity field in the upper layer. Comparisons of the velocity field at successive times for a single experiment gave the rate of decay of the vorticity in the eddy.

3.2. *Eddy stability*

Under some initial conditions an eddy becomes unstable with the vortex breaking down into several baroclinic eddies in the manner reported by Saunders (1973) and Griffiths & Linden (1981); we wanted to avoid such conditions. Saunders created baroclinic eddies on a horizontal bottom by filling a cylinder to a depth H with salt solution, and then removing the cylinder. The heavy fluid then spread under the fresh water having the same depth H. The resulting circular eddy was stable if the

parameter $F_0 = g'H/f^2R_0^2$ exceeded a critical value of $F_0 = 1.8$. In similar experiments, Griffiths & Linden (1981) released fluid that was less dense than the surrounding fluid and which spread out under the free surface. The ratio δ_0 of the initial depth H_0 of buoyant fluid in the cylinder to the total water depth H was also varied. In this case, all eddies were unstable, the difference with Saunders' results being attributed to different effects of friction at the rigid bottom and the free surface.

For the present experiments with a sloping bottom a depth ratio $\delta_0 = H_0/H$ in the range 0.2–0.5 was chosen. We verified that stable eddies are found when $F_0 = g'H\delta_0/f^2R_0^2 > 2$. All of the following experiments were conducted under stable conditions. For example, experiments with $\delta_0 \approx 0.3$ and $\delta_0 \approx 0.5$ had initial Froude numbers $F_0 \approx 2.5$ and $F_0 \approx 5$ respectively.

3.3. *Qualitative observations*

Photographs of the flow pattern at successive times during a single experiment are shown in figure 3 (plates 1 and 2). The time elapsed after removing the cylinder is non-dimensionalized by the period of rotation of the tank ($T = 4\pi/f$). In this experiment, the fresh water above the lens is coloured with green–yellow fluoresceine dye, and the dense water beneath is shown using blue dye. The initial position of the centre of the cylinder is marked in figure 3 (*b–e*) by a star, from which the displacement of the eddy can be seen. Within a single rotation period following removal of the cylinder, the formation of a single coherent vortex is clear. Weak shear instabilities occur at the edge of the vortex during the initial evolution towards geostrophic equilibrium. However, the motions induced by these small-scale instabilities dissipate within two or three rotation periods. A more important initial effect is the force of gravity which pushes the lens downhill, and which contributes to the generation of the strong cyclonic vorticity above the lens. But an uphill 'northward' motion commences within about one rotation period, and this is accompanied by an outwards mass flux from the Ekman layer.

Apart from the observation that a single stable baroclinic eddy can be produced on a sloping bottom, the most significant feature of the time evolution of the system is the monotonic 'westward' and 'northward' (uphill) drift of the lens after the short initial adjustment period (figure 3*b–e*). The translation speed of the lens is found to be very small compared with the translation speed of isolated eddies in a deep ocean, (2.7), approximately 1 mm s^{-1} compared with about 1 cm s^{-1}, and the 'northward' speed is of the same order of magnitude as the 'westward' speed. The side views in figure 3 show that the displacement of the fluoresceine-marked water volume in the upper layer is identical with the displacement of the dense lens (above the Ekman layer), indicating that most of the water that was initially at rest above the dense fluid is trapped in a Taylor column above the lens. In our notation the necessary condition for the occurrence of Taylor columns above a rigid topography (Ingersoll 1969; Hogg 1973; Huppert 1975; McCartney 1975):

$$\delta \gtrsim \frac{C_x}{fL}, \tag{3.2}$$

is obviously satisfied in our experiment ($C_x \approx 1$ mm s^{-1}, $L \approx 10$ cm, $f \approx 1$ s^{-1}, $\delta_0 = O(1)$). A mass flux out of the Taylor column is also visible on figure 3 (*b–e*), where the fluoresceine dye marks a tail that extends behind the eddy. This tail may indicate a weak topographic Rossby wave behind the eddy – another indication that our eddy is not isolated. Another view (figure 4) clearly indicates the coherency of the eddy above the Ekman layer.

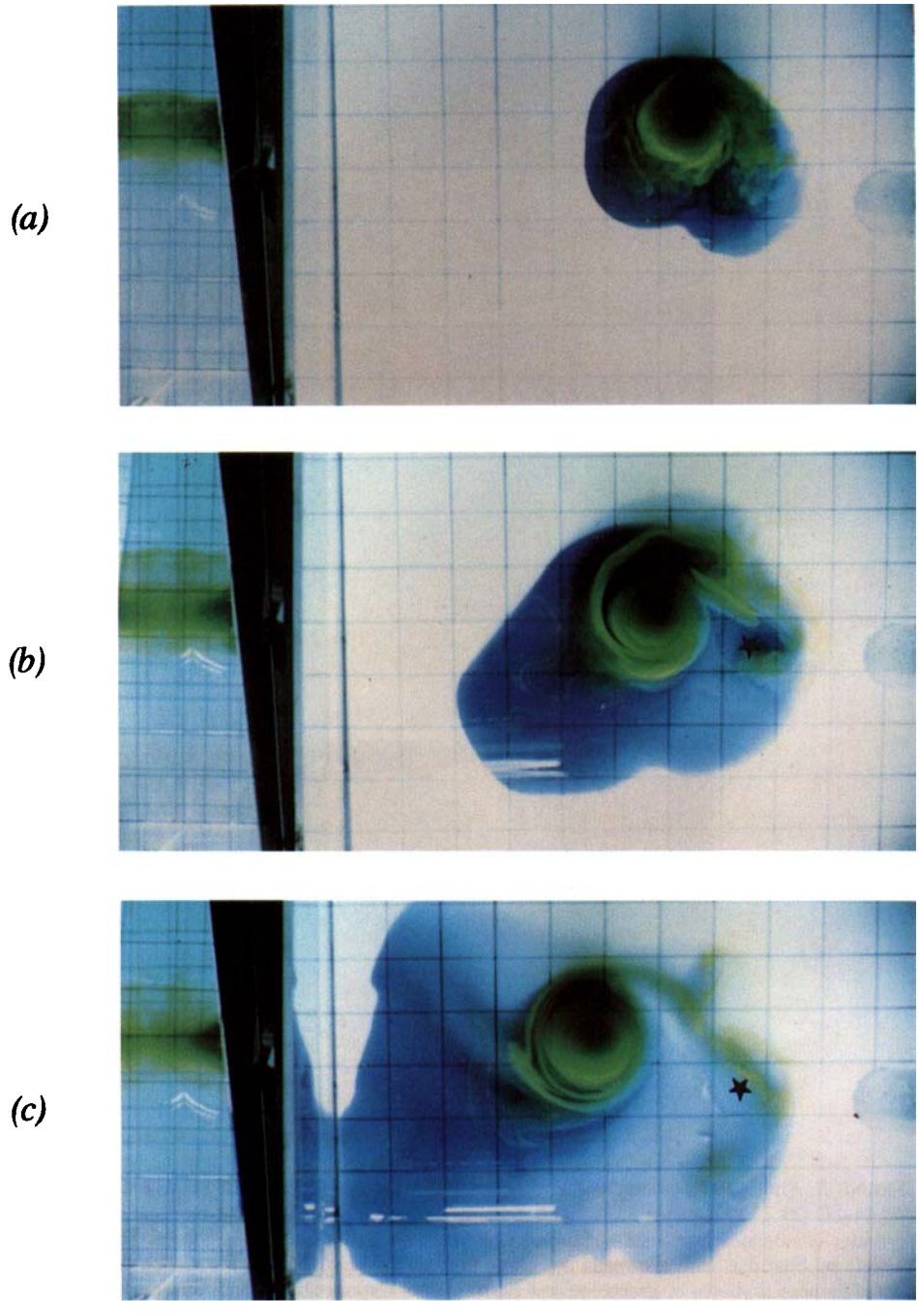

FIGURE 3 (a–c). For caption see Plate 2.

(d)

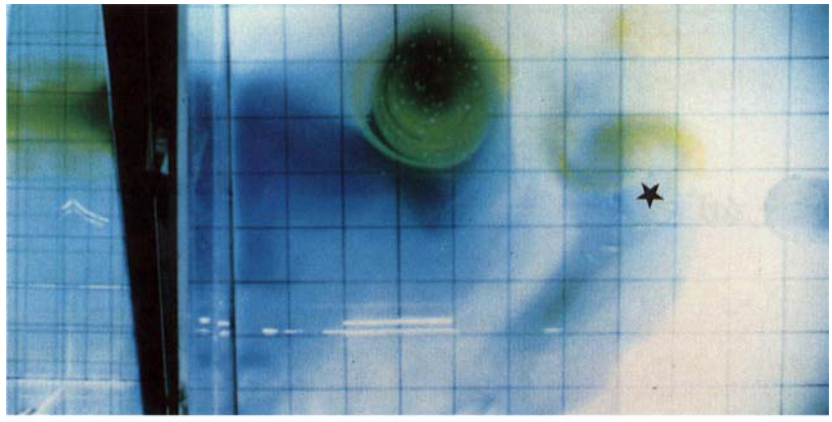

(e)

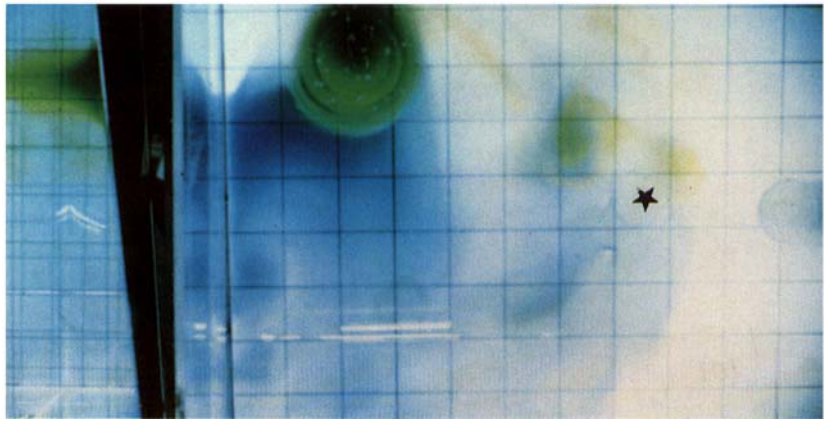

FIGURE 3. Photographs showing the time evolution of an eddy structure at times *(a)* 1.2*T*, *(b)* 7.1*T*, *(c)* 14.2*T*, *(d)* 23.7*T* and *(e)* 33.1*T*, with *T* being the period of rotation of the tank. Initial position of the cylinder is indicated by the star. Plan and side views are given for each exposure. The dense fluid is made visible by blue dye which spreads out along the bottom in an Ekman layer. The fresh water initially on top of the lens is shown by green–yellow fluoresceine. Experimental conditions are: bottom slope $s \approx 0.14$, $f \approx 1.01\ \mathrm{s}^{-1}$, $g' \approx 6.5\ \mathrm{cm\ s}^{-2}$, $\delta_0 \approx 0.5$, $F_0 \approx 4.1$. Direction of rotation is anticlockwise. In the plan view leftwards corresponds to 'westward'.

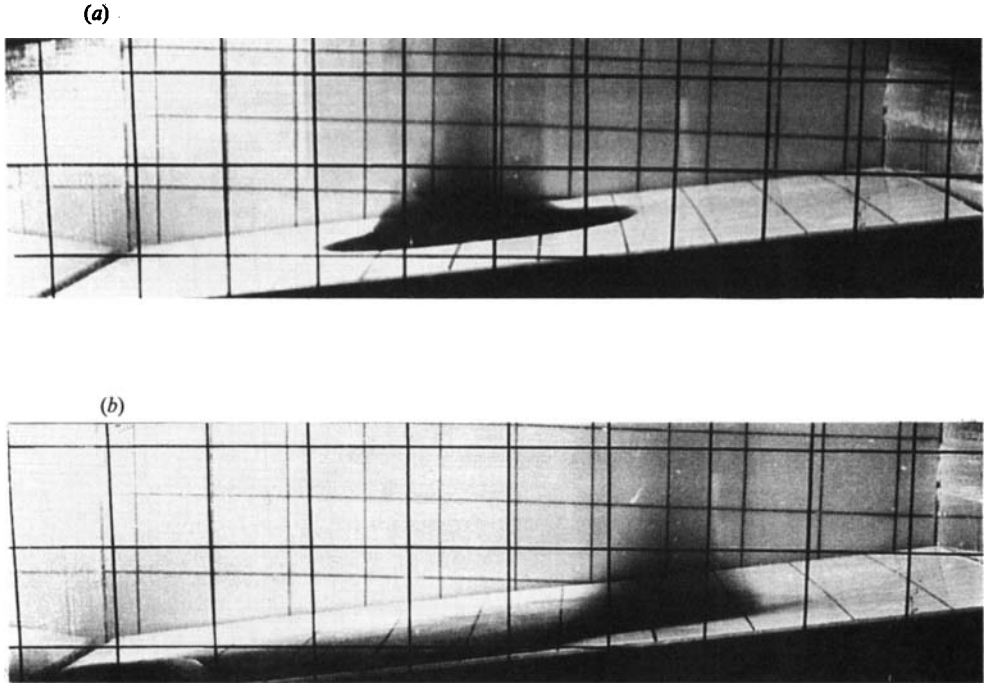

FIGURE 4. Side-view photographs of the lens at two successive times (2.1 and 21.1 rotation periods for (*a*) and (*b*) respectively). Experimental conditions are: $s \approx 0.14$, $f \approx 0.9\ \mathrm{s}^{-1}$, $g' \approx 6\ \mathrm{cm\ s}^{-2}$, $\delta_0 \approx 0.5$.

When the eddy comes into the vicinity of the wall, the drift speed of the eddy decreases and a complicated interaction ensues. In some cases the eddy was observed to stay trapped in the vicinity of the wall or move downhill alongside the wall. In other cases the eddy became unstable.

The effect of the centrifugal force has to be reduced as much as possible. The necessary condition for the centrifugal force to be small compared with the Coriolis force is $(\Delta\rho/\rho)(fD/4C_x) \ll 1$ (where D is the distance from the centre of the eddy to the axis of rotation). The latter ratio varies from 0.1 at the beginning of each experiment to 0.5 when the eddy is close to the wall. While these are not very small values, we believe that centrifugal forces are not sufficiently strong to play a major role in the experiment.

3.4. *The displacement of eddies*

The position of the centre of each eddy as a function of time is plotted in figure 5 for five experiments. The parameters for the experiments are listed in table 1. The initial relative depths δ_0 of the dense fluid contained in the cylinder range from 0.35 to 0.55, and the initial Froude numbers ($F_0 = g'H\delta_0/f^2R_0^2$) lie between 2.4 and 5.2. All of these eddies are stable. In most experiments the flow field in the upper layer was observed from the displacement of paper pellets on the free surface and the centre of the vortex in the upper layer was readily determined. In one of these experiments, the upper-layer vortex contained fluoresceine dye and the vortex centre was determined as the centre of the circular patch of dye. The time interval between successive measurements of the position of the vortex is one minute, and corresponds to between four and six rotation periods of the tank. Some intermediate positions

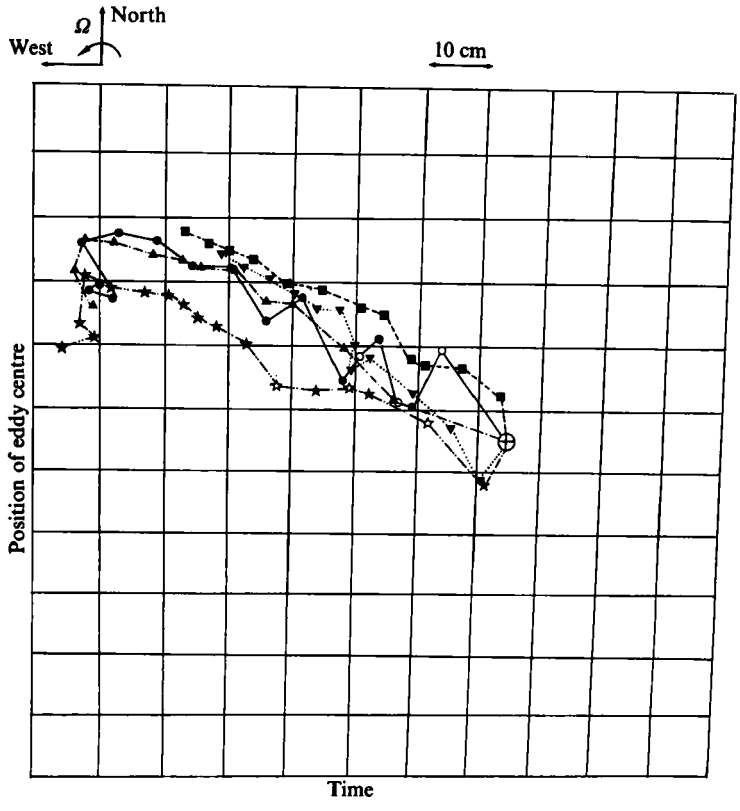

FIGURE 5. Displacements of the centre of baroclinic eddies with time in five experiments. Experiment parameters are listed in table 1. The initial position of the lens is marked by ⊕ (but the initial motion is not shown on this diagram). The time interval between two successive points is generally 1 min (4–6 rotation periods of the tank). When intermediate positions (30 s apart) are given, the symbol is open. The upslope direction is 'northward'. The scale is given by the painted grid on the bottom plate.

(30 s after the previous point) are also plotted, in which case the symbol is open. The initial position of the cylinder is the same for all five experiments. The distortion of the 10 cm scale grid painted on the bottom slope is due to the camera position.

All eddies display a slow continuous westward translation. A northward displacement is also clear, and is one-third to one-half of the westward displacement. Large-amplitude uphill–downhill oscillations were observed in one experiment, although no special perturbation was noticed during the releasing of the fluid. The lack of temporal resolution precludes estimation of their frequency. The behaviour very shortly after release is not seen in figure 5 since the first measurements are taken three to six rotation periods after removal of the cylinder. More careful observations of the release show that a rapid upslope motion follows the initial downhill spreading of the lens during the first couple of rotation periods. Three of the five experiments were observed over a sufficiently long time to see the interaction of the eddy with the wall. In these three cases the structure moved downhill beside the wall. During the intervening time of 30–50 rotation periods, the evolution appeared to be little influenced by either the boundaries or the initial unsteady processes. Westward and

	Experimental conditions					Translation			Vortex structure		
symbol	f (s^{-1})	g' (cm s^{-2})	H (cm)	δ_0	F_0	C_i (mm s^{-1})	C_x (mm s^{-1})	C_y (mm s^{-1})	ω/f	r_0 (cm)	$\frac{\tau f}{4\pi}$
▲	1.1	6.5	25	0.35	2.4	−8.3	−0.95 ±0.30	0.55 ±0.45	0.74	3.2	40
▼	1.0	4.5	26	0.55	3.1	−6.3	−0.60 ±0.30	0.45 ±0.30	—	—	—
●	1.0	6.5	26	0.5	4.1	−9.1	−0.95 ±0.05	0.55 ±1.0	—	—	—
★	0.9	6	26	0.5	4.6	−9.4	−0.80 ±0.30	0.35 ±0.35	—	—	—
◆	0.9	5.6	25	0.5	4.6	—	—	—	0.71	3.4	40
■	0.9	6	26	0.55	5.2	−9.4	−0.75 ±0.20	0.35 ±0.30	1.01	3.3	19

TABLE 1. Parameters for the experiments plotted in figure 5, along with the measured translation speeds C_x and C_y, the theoretical westward translation speed C_i, the maximum relative vorticity ω/f in the upper-layer vortex (see figure 8), vortex core r_0 of the vortex above the lens and the e-folding decay time τ for the upper-layer vorticity (non-dimensionalized with the rotation period of the tank). Properties of the upper-layer vortex were measured for three experiments only.

northward translation speeds $-C_x$ and C_y, respectively, during that interval were estimated and the results are shown in table 1. Also shown in table 1 are the westward propagation speeds C_i (2.7) predicted for isolated eddies. Measured values of the westward translation speed lie between 0.5 and 1 mm s^{-1}. These values are an order of magnitude smaller than C_i.

3.5. *The vortex flow structure above the lens*

The vortex located on top of the lens warrants special attention. The motion of the pellets on the free surface is observed to be axisymmetric to within a very good approximation, and the velocities far from the eddy centre are very small. The axisymmetry enables the centre of the vortex and the azimuthal component of velocity as a function of radius to be readily determined after digitizing the particle positions and displacements.

Radial profiles of the azimuthal velocity at four successive times during two experiments are presented in figures 6 and 7. Comparison of the profiles for successive exposure times shows a decrease of the strength of the vortex with time. No significant increase in the size of the vortex is apparent.

In order to estimate the vorticity ω at the centre of the vortex and the radius r of the vortex core, a classical Rankine vortex model,

$$\left.\begin{aligned} V_\theta^0(r) &= \tfrac{1}{2}\omega r \quad \text{for } r < r_0, \\ V_\theta^0(r) &= \tfrac{1}{2}\omega \frac{r_0^2}{r} \quad \text{for } r > r_0, \end{aligned}\right\} \tag{3.3}$$

was fitted to the experimental data, and is shown in figures 6 and 7. It provides a reasonable description of the data but we notice that measured velocities decay faster than the Rankine profile at large radii. This indicates anticyclonic vorticity surrounding the vortex core. The lengthscale r_0 of the vortex core, determined by

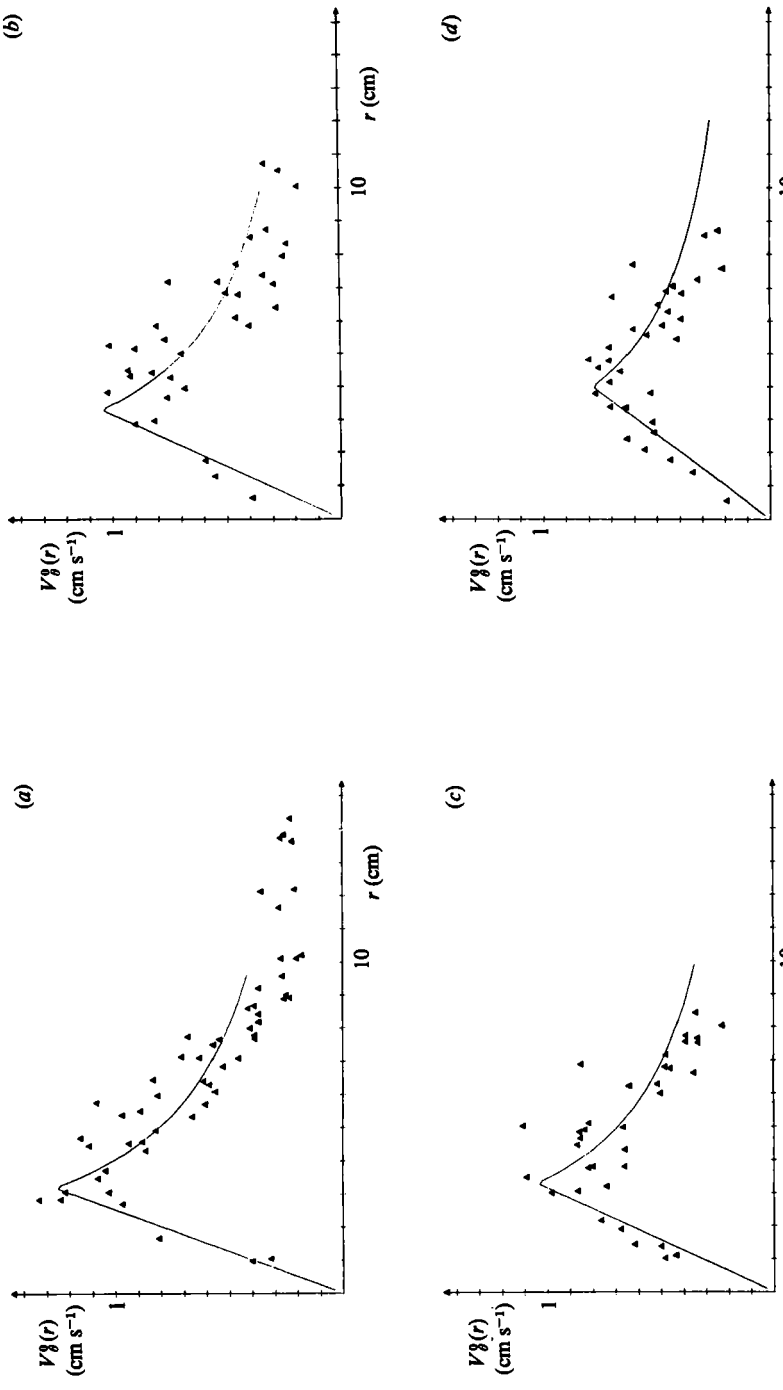

FIGURE 6. Azimuthal component of the velocity in the upper layer as a function of distance from the centre of the vortex. A theoretical profile (given by (3.3)) is shown by the continuous lines. Parameters are: $g' \approx 6.5$ cm s^{-2}, $f \approx 1.1$ s^{-1}, $\delta_0 \approx 0.35$. The respective times for (*a*), (*b*), (*c*), (*d*) are 15.3, 20.3, 25.4 and 30.5 rotation periods of the tank.

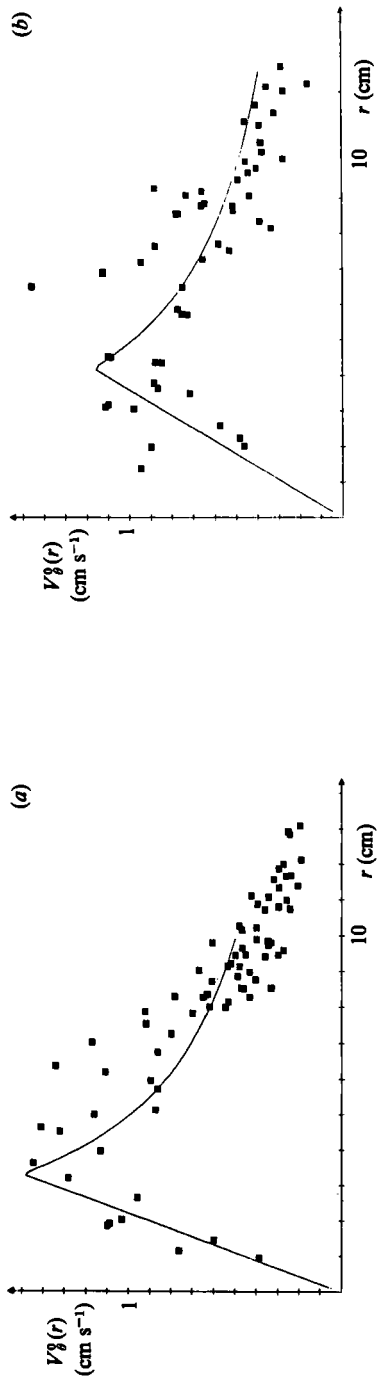

FIGURE 7. Azimuthal component of the velocity in the upper layer for a second experiment. Parameters are: $g' \approx 6$ cm s^{-2}, $f \approx 0.9$ s^{-1}, $\delta_0 \approx 0.55$. The respective times for (*a*), (*b*), (*c*), (*d*) are 21, 25.2, 29.4 and 33.6 rotation periods of the tank.

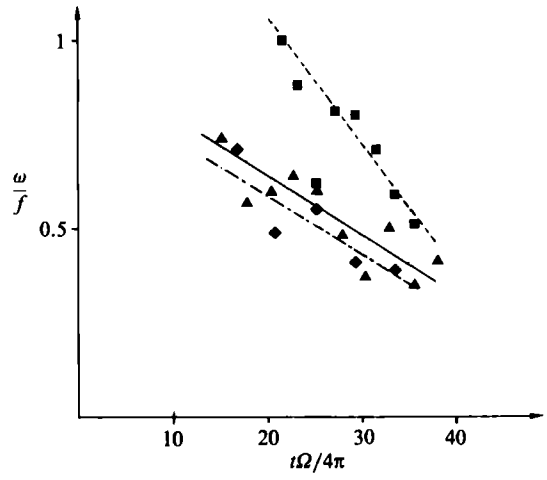

FIGURE 8. Evolution of the vorticity ω at the centre of the vortex in the upper layer for three experiments. Parameters for the experiments are listed in table 1. Vorticity ω is non-dimensionalized by the background vorticity f and time is non-dimensionalized by the rotation period of the tank $4\pi/f$. Straight lines fit the data for each experiment.

fitting (3.3) to the velocity data, is given in table 1. This lengthscale does not vary significantly from one experiment to another.

The evolution of the vorticity ω at the centre of the vortex is shown in figure 8, where the ratio of ω to the Coriolis frequency f is plotted as a function of dimensionless time $tf/4\pi$. Data are plotted for three experiments the parameters of which are shown in table 1. From the straight-line fits included in figure 8, a characteristic e-folding time τ for decay of the vorticity inside the eddy is deduced. This decay time is given in table 1, non-dimensionalized by the rotation period $4\pi/f$ of the tank. For all cases considered, decay time was found to be very long, indicating that the effects of decay on the vortex dynamics are small. Note that these times are notably larger than the Ekman decay time

$$\tau_{\mathrm{E1}} \sim H \frac{1}{(2\nu f)^{\frac{1}{2}}} \tag{3.4}$$

based on the maximum thickness H. The longer experimental decay time may be attributed to the fact that the kinetic energy in the upper layer is shielded from the rigid boundary by the lens. Another possible reason is related to the available potential energy (Stern 1975*b*, p. 86). Of great significance is the observation that the vortices are intense, and in all experiments the ratio of the relative vorticity ω to the background vorticity f is of order one. The concentration of such a strong vorticity requires a complex adjustment process including significant three-dimensional motions. An inviscid stretching of fluid columns above the lens cannot account alone for the vorticity concentration achieved in the experiments. The conservation of potential vorticity requires the depth of fluid columns to increase by a factor of two in order to produce a relative vorticity of order f, so that the lens should be completely flattened or it should move far downhill. Neither of these scenarios corresponds to the experimental results.

4. The north-westward motion of the eddies

4.1. *The balance of forces acting on the lens*

An understanding of the experiment requires an examination of the balance of forces acting on the lens (see (2.5) and (2.6)), in order to explain how the buoyancy force is balanced. This requires an estimate of the relative importance of global forces, including the Coriolis force due to the displacement of the lens, the pressure force applied by the vortex above the lens and the buoyancy downhill force. With the geostrophic scaling,

$$\left.\begin{gathered}(x,y)\sim L,\quad (u_1,v_1)\sim V,\quad (u_2,v_2)\sim V,\\ h_2\sim \delta H,\quad h_1\sim (1-\delta)H,\\ C_x\sim \frac{g's}{f},\quad p_1\sim \rho fVL,\quad p_2\sim \rho fVL,\end{gathered}\right\} \tag{4.1}$$

we have four non-dimensional numbers, namely the Rossby number $\epsilon = V/fL$, the Froude number $F = g'H/f^2L^2$ (with $g' = \Delta\rho g/\rho$), the slope parameter $\beta = sL/H$ and the relative depth of the dome δ. Assuming that the effect of the slope is small we have $\beta \ll 1$, but the relative depth of the dome δ as well as the Rossby number ϵ are $O(1)$. The flow can be examined by an expansion of the flow field in the small parameter β, in the manner previously used by Killworth (1983) and Flierl (1984), namely

$$\left.\begin{gathered}u_1 = u_1^0+\beta u_1^1+\ldots,\quad v_1 = v_1^0+\beta v_1^1+\ldots,\\ u_2 = \beta u_2^1+\ldots,\quad v_2 = \beta v_2^1+\ldots,\\ p_1 = p_1^0+\beta p_1^1+\ldots,\quad p_2 = \beta p_2^1+\ldots,\\ h_2 = h_2^0+\beta h_2^1+\ldots.\end{gathered}\right\} \tag{4.2}$$

The expansion is similar to those that were carried out by the authors just cited, but it is worth noting that the expansion is applied to a different physical problem. In Killworth's and Flierl's models ageostrophic large-amplitude motions were confined within lenses of finite volume (allowing maximum velocity at the edge of the lenses), whereas in our problem motions are small in the lens and ageostrophic motions take place in the surrounding fluid. Though velocity measurements inside the lens were unobtainable, we assume on theoretical grounds that velocities inside the dome are small since the Ekman friction decreases the magnitude of motion in the lens within a few rotation periods. This effect is substantiated in §4.2 and we shall see there that the slow uphill translation implies a relative vorticity of order 0.1 in the lens. The buoyancy force is of order β, and we need an accurate description of the flow above the lens to this order. Since the measured translation speeds C_x are much smaller than C_1, (2.7), the effect of the Coriolis force is at most of order β^2, and can be neglected. Equation (2.6) then reduces to

$$\iint_{\mathscr{S}} h_2^0\,\partial_y p_1^0\,\mathrm{d}x\,\mathrm{d}y = 0 \tag{4.3}$$

and

$$-\epsilon\iint_{\mathscr{S}}(h_2^1\,\partial_y p_1^0+h_2^0\,\partial_y p_1^1)\,\mathrm{d}x\,\mathrm{d}y - F\iint_{\mathscr{S}} h_2^0\,\mathrm{d}x\,\mathrm{d}y = 0, \tag{4.4}$$

at zero and β-order, respectively.

We verify (4.3) by observing that, since p_2 is of order β, (4.2), the hydrostatic relation (2.2) is at zero order

$$\epsilon \partial_y p_1^0 + F\delta \partial_y h_2^0 = 0. \tag{4.5}$$

The integral on the left-hand side of (4.3) then becomes

$$-\iint_{\mathscr{S}} \frac{F\delta}{\epsilon} \partial_y (\tfrac{1}{2} h_2^{02}) \, dx \, dy,$$

which is zero by Stokes theorem. In order to compare this with experiments, we specify the flow in the upper layer to be axisymmetric at zero order (i.e. $h_2^0(r)$, $V_\theta^0(r)$, where $V_\theta^0(r)$ is the azimuthal velocity component as defined in §3). The momentum equation in the upper layer is then written at zero order as

$$V_\theta^0 + \epsilon \frac{V_\theta^{02}}{r} = -\frac{F\delta}{\epsilon} \partial_r h_2^0, \tag{4.6}$$

and $h_2^0(r)$ is assumed to vanish on the circle $r = 1$ ($h_2^0(1) = 0$).

The specification of p_1^1 and h_2^1 is required to verify (4.4), the balance of forces at β-order. However, we observe that the particular solution,

$$p_1^1 \equiv 0, \quad h_2^1 \equiv -\frac{1}{\delta} y \tag{4.7}$$

verifies (4.4). An integration by parts with respect to y of the first term of (4.4) shows that this term is of opposite sign to the second term. The domain of integration is here the disk of radius $r = 1$. This differs from the area $\mathscr{S}$ covered by the lens in the plane (x, y) as defined in §2. Indeed, the shape of the lens is

$$h_2(x, y) = h_2^0(r) - \frac{\beta}{\delta} y. \tag{4.8}$$

Since the eddy is not isolated ($V_\theta^0(1) \neq 0$), (4.6) implies $\partial_r(h_2^0)(1) \neq 0$, and the edge of the lens is given by (r, θ)-solution of

$$(r-1) \partial_r h(1) - \frac{\beta}{\delta} \sin\theta = 0. \tag{4.9}$$

The displacement of the edge of the lens from the circle $r = 1$ is of order β. The depth of the lens is of order β in the region of displacement of the edge, and therefore the difference between $\mathscr{S}$ and the disk of radius $r = 1$ contributes only to order β^2 in the integrated momentum. This justifies considering the disk of radius $r = 1$ as the area covered by the lens when solving (4.3) and (4.4).

An interesting property of the simple solution (4.7) is that the zero-order axisymmetric upper-layer flow follows the lines of constant depth above the lens because

$$h_1^0 + \beta h_1^1 = 1 - \delta h_2^0 - \beta\delta h_2^1 - \beta y = 1 - \delta h_2^0(r). \tag{4.10}$$

Such a flow is certainly not far from being realized in the experiment as our observations show very axisymmetric streamlines. Equation (4.4) indicates that this flow applies a net pressure force on the lens, owing to the modification of the shape of the lens h_2^1, which balances the buoyancy. The zero-order axisymmetric velocity was measured in the experiments, and (4.6) allows the determination of the amount of vorticity in the upper layer that is necessary to maintain a given amount of dense

water. Integration of (4.6) relates the volume of the lens to the velocity distribution V_θ^0. In dimensional form we have

$$-\pi\int_0^L r^2\left(fV_\theta^0+\frac{V_\theta^2}{r}\right)\mathrm{d}r = g'\pi\int_0^L r^2\,\partial_r h_2^0\,\mathrm{d}r = -2\pi g'\int_0^L rh_2^0\,\mathrm{d}r, \tag{4.11}$$

where L denotes the distance of the edge from the centre of the dome. The right-hand side of (4.11) is the total volume of the lens. The distance L has been computed from (4.11) with the velocity profile (3.3), the total volume being determined from the initial conditions. The result predicts a radius of the correct order of magnitude, though the lenses have flatter shapes than is observed in the experiments. For the two experiments plotted in figures 6 and 7 ($F_0 = 2.4$ and 5.2, respectively) the corresponding values of L are 22 and 27 cm, respectively. The maximum depths at the centre of the lens are then 1.9 and 2.3 cm for the two cases. The shapes would be somewhat steeper when taking into account the anticyclonic motions in the lens. We nevertheless believe that the solution given here corresponds to an asymptotic case towards which the eddies observed in the experiment evolve.

Finally, it is worth noting that the flow described in this section does not verify the integral theorem (2.8). At the edge of the eddy ($r = 1$), the existence of motions ($V_\theta^0(1) \neq 0$) implies non-zero pressures at $r = 1$, and (4.5) implies

$$\epsilon p_1^0 + F\delta h_2^0 = A, \tag{4.12}$$

where A is a negative constant. Outside the eddy the pressure p_1 increases towards O so that the integral (2.8) is negative if it converges.

4.2. *The effect of Ekman friction and the displacement of the lens*

Figure 5 shows that for all experiments the lens and the eddy follow a north-westward path and the lens is eventually carried to positions that are higher on the slope than the initial position. Because the centrifugal force is negligible, the increase of absolute kinetic energy associated with the strong cyclonic motions in the upper layer implies that a significant amount of potential energy is released. Since part of the initial dense water moves uphill with the lens, another part of the dense fluid must flow downhill outside the lens. We observe this in figures 3 and 4 as a flow in a thin bottom layer moving south-westward. This flow is a result of Ekman pumping within the lens. A sketch of the lens and the eddy is drawn in figure 9 and the Ekman circulation is depicted. A typical non-dimensional time scale τ_{E2} for the Ekman decay of the lens is

$$\tau_{E2}\frac{f}{4\pi} \sim \frac{\delta_0 H}{4\pi}\left(\frac{f}{2\nu}\right)^{\frac{1}{2}}. \tag{4.13}$$

The approximate experimental value of this number is 3. This is an order of magnitude smaller than the timescale of decay of the vortex on top of the lens (see table 1). The vertical velocities produced by Ekman pumping would tend to decrease the height of the lens at the rate

$$\partial_t h_2 \sim \left(\frac{\nu}{2f}\right)^{\frac{1}{2}}\xi, \tag{4.14}$$

where ξ is the vorticity of the flow inside the lens. We estimate $\xi \sim -\frac{1}{2}f$ because the heavy fluid collapses by a factor of two after release, and therefore the order of magnitude of the velocity $\partial_t h_2$, (4.14), is 0.3 mm s^{-1}. Acting alone this effect would produce a significant stretching of the eddy above the lens. The vorticity in the upper layer would increase in time. Since the depth above the lens is smaller on its uphill

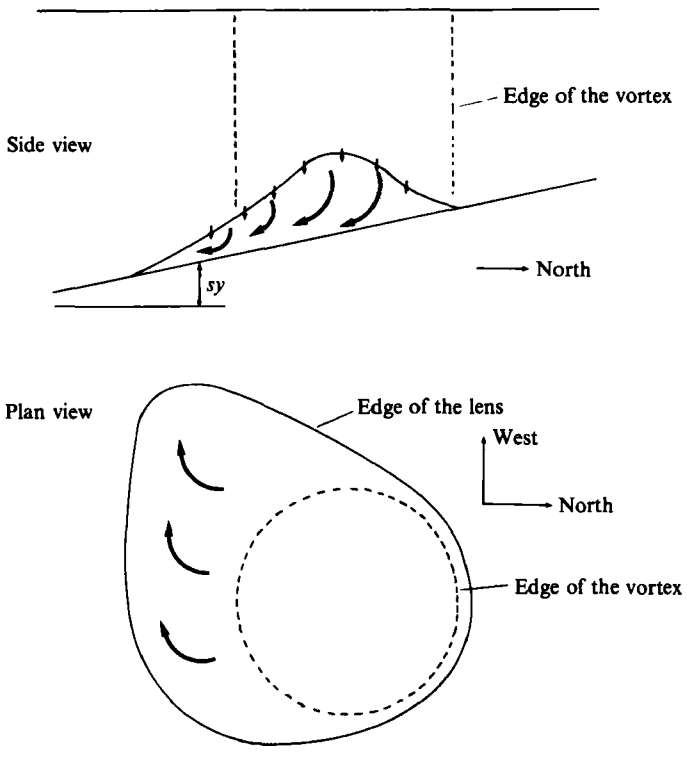

FIGURE 9. A sketch of the lens and the Taylor column both in plane and side views. Large arrows indicate the Ekman pumping motion in the lens. The depth of the lens decreases with time as indicated by the small arrows on the interface.

side the stretching is more efficient on that side, producing smaller pressures north of the lens. The lens is therefore pushed uphill in order to offset the stretching, to offset the increase in ω, and to restore the approximate balance between the pressure force and gravity. The uphill velocity necessary to offset (4.14) is

$$C_y \sim -\frac{1}{s}\left(\frac{\nu}{2f}\right)^{\frac{1}{2}}\xi \sim \frac{1}{s}\left(\frac{\nu}{2f}\right)^{\frac{1}{2}}\tfrac{1}{2}f, \tag{4.15}$$

the experimental value of which is ≈ 2.5 mm s^{-1}. Such a velocity does occur at the beginning of the experiment even though smaller values occur at later times (table 1). The reason is that the vorticity ξ within the lens decreases in time producing a decrease of the northward translation of the lens. In fact a rapid decrease of the northward speed is observed in the experiment (see figure 5). Note that the typical value $C_y \sim 0.5$ mm s^{-1} corresponds to a characteristic relative vorticity $\xi/f \sim 0.1$ in the lens (equation (4.15)).

Part of the northward movement of the lens might also be attributed to weak radiation of Rossby waves (McWilliams & Flierl 1979) or other inertial wake effects that cause the energy of the cyclonic vortex to decrease. As the cyclonic vorticity decreases the conservation of potential vorticity requires the column thickness to decrease via a northward motion. We were not able to provide a quantitative estimate of the importance of this second mechanism, but our analysis of the experiment indicates that it is at most as important as the effect of Ekman friction.

5. Summary

In this paper we have addressed the question of the existence and the realizability of a baroclinic isolated eddy on a sloping bottom in a rotating fluid. When the depths of the lens and of the surrounding layer have the same order of magnitude, a general integral requirement leads to the surprising conclusion that an isolated dense lens on a sloping bottom can exist only if there are strong cyclonic motions above it.

Coherent and long-lived eddies have been produced on a sloping bottom. They have very strong cyclonic motion above the lens of dense water. In order to avoid baroclinic instability and vortex splitting the lateral scale of these eddies had to be kept small, of the order of the internal radius of deformation. The dome as well as the Taylor column above it display a slow westward and uphill drift. An analysis of the implications of the isolation requirements (§2), which is compared with the experiments, leads us to conclude that our coherent eddies are not isolated. In particular they do not satisfy the integral requirement (2.8). Moreover, an isolated eddy propagates with the speed of isolated eddies in an infinitely deep and motionless ocean (Nof 1983) even in the presence of strong motion above the lens. This implies that the vortex on top of the lens applies no net pressure on the lens. The translation speed of an isolated eddy is much larger than the translation speeds of the eddies produced in the laboratory. We conclude that for the laboratory vortices the buoyancy force is balanced by the pressure force applied by the vortex. A simple model is given, in which the streamlines in the upper layer follow the lines of constant depth, and we show that the strength of the vortices in the experiment is sufficient to account for the balance of buoyancy, Finally, the effect of Ekman friction is examined and we demonstrate that this phenomenon can account for the northward displacement of the eddy.

The work was initiated during the 1983 Geophysical Fluid Dynamics Program, where discussions with G. R. Flierl were particularly valuable. J. A. Whitehead and R. Frazel of the Woods Hole Oceanographic Institution made possible preliminary experiments. Further experiments were conducted at the Institut de Mécanique de Grenoble with the assistance of S. Layat. M.M. thanks J. Verron and B. Barnier for helpful comments and E. J. Hopfinger for his continuous support. The work of M.M. was supported in 1984–5 by the CNEXO under contract number 84/3276. The work of M.E.S. was partially supported by O.N.R. and a visiting professorship from the Institut de Mécanique de Grenoble.

REFERENCES

FLIERL, G. R. 1979*a* Baroclinic solitary waves with radial symmetry. *Dyn. Atmos. Oceans* **3**, 15–38.

FLIERL, G. R. 1979*b* A simple model of the structure of warm and cold-core rings. *J. Geophys. Res.* **84**, 781–785.

FLIERL, G. R. 1984 Rossby wave radiation from a strongly nonlinear warm eddy. *J. Phys. Oceanogr.* **14**, 47–58.

FLIERL, G. R., STERN, M. E. & WHITEHEAD, J. A. 1983 The physical significance of modons. *Dyn. Atmos. Oceans* **5**, 1–41.

GRIFFITHS, R. W., KILLWORTH, P. D. & STERN, M. E. 1982 Ageostrophic instability of ocean currents. *J. Fluid Mech.* **117**, 343–377.

GRIFFITHS, R. W. & LINDEN, P. F. 1981 The stability of vortices in a rotating stratified fluid. *J. Fluid Mech.* **105**, 283–316.

HOGG, N. G. 1973 On the stratified Taylor column. *J. Fluid Mech.* **58**, 517–537.

HOUGHTON, R. W., SCHLITZ, R., BEARDSLEY, R. C., BUTMAN, B. & CHAMBERLIN, J. C. 1982 The middle Atlantic Bight cold pool: evolution of the temperature structure during summer 1979. *J. Phys. Oceanogr.* **12**, 1019–1029.

HUPPERT, H. E. 1975 Some remarks on the initiation of inertial Taylor columns. *J. Fluid Mech.* **67**, 397–412.

INGERSOLL, A. P. 1969 Inertial Taylor columns and Jupiter's Great Red Spot. *J. Atmos. Sci.* **26**, 744–752.

KILLWORTH, P. D. 1983 On the motion of isolated lenses on a beta-plane. *J. Phys. Oceanogr.* **13**, 368–376.

MCCARTNEY, M. S. 1975 Inertial Taylor columns on a β-plane. *J. Fluid Mech.* **68**, 71–95.

MCWILLIAMS, J. C. & FLIERL, G. R. 1979 On the evolution of isolated, nonlinear vortices. *J. Phys. Oceanogr.* **9**, 1155–1182.

MORY, M. 1983 Theory and experiment of isolated baroclinic vortices. *Tech. rep.* WHOI-83-41, 114–132. Woods Hole Oceanographic Institute.

MORY, M. 1985 Integral constraints on bottom and surface isolated eddies. *J. Phys. Oceanogr.* **15**, 1433–1438.

NOF, D. 1983 The translation of isolated cold eddies on a sloping bottom. *Deep-Sea Res.* **30**, 171–182.

NOF, D. 1984 Oscillatory drift of deep cold eddies. *Deep-Sea Res.* **31**, 1395–1414.

NOF, D. 1985 Joint vortices, eastward propagating eddies and migratory Taylor columns. *J. Phys. Oceanogr.* **15**, 1114–1137.

RING GROUP 1981 Gulf Stream cold-core rings: their physics, chemistry and biology. *Science* **212**, 1091–1100.

SAUNDERS, P. M. 1973 The instability of a baroclinic vortex. *J. Phys. Oceanogr.* **3**, 61–65.

SMITH, P. C. 1976 Baroclinic instability in the Denmark strait overflow. *J. Phys. Oceanogr.* **6**, 355–371.

STERN, M. E. 1975*a* Minimal properties of planetary eddies. *J. Mar. Res.* **33**, 239–267.

STERN, M. E. 1975*b* *Ocean circulation Physics.* Academic.